https://doi.org/10.1016/j.ijhydene.2020.07.155

Dynamic Behaviour and Control Strategy of High Temperature Proton Exchange Membrane Electrolyzer Cells (HT-PEMECs) for Hydrogen Production

Dongqi Zhao[a,b], Qijiao He[b], Jie Yu[b], Jianhua Jiang[a], Xi Li[a]*, Meng Ni[b]*

a. School of Artificial Intelligence and Automation, Key Laboratory of Image Processing and Intelligent Control of Education Ministry, Huazhong University of Science and Technology, Wuhan, Hubei, China.

b. Building Energy Research Group, Department of Building and Real Estate, The Hong Kong Polytechnic University, Hung Hom, Kowloon, Hong Kong.

*Corresponding author: Xi Li and Meng Ni.

E-mail address: lixi_wh@126.com (Xi Li), meng.ni@polyu.edu.hk (Meng Ni).

Abstract

A fast and safe dynamic process is a key issue during the start-stop and adjustment of high-temperature proton exchange membrane electrolyzer cells (HT-PEMECs). In the paper, a 2D multi-physics model is developed to investigate the dynamic process in an HT-PEMEC. First, the dynamic responses of step scheme, multistep scheme and diagonal scheme are compared. It is found that the step scheme has the fastest dynamic response, but it may cause the problem of reactant starvation. The dynamic response speed of diagonal scheme is slower than the step scheme, but it can prevent the problem of reactant starvation. Subsequently, the dynamic process is optimized with a fast dynamic response without reactant starvation. This paper proposes a fast and safe dynamic process adjustment scheme and forms a basis for subsequent control of the HT-PEMEC stack and system.

Keywords: Hydrogen Production; Electrolysis; Proton exchange membrane electrolyzer cell; Numerical modelling; Dynamic response; Optimization problem.

1. Introduce

Renewable energy technology is critical to solving the global environmental pollution problems and energy shortage. Renewable energy sources such as tidal energy, solar energy and wind energy are site-specific, intermittent and therefore unreliable. Therefore, effective energy storage is essential for a wide and reliable application of renewable energy technology. Hydrogen is an environmentally friendly fuel. Using excess renewable power to drive water electrolyzers for water-splitting is a promising method for storing the excess renewable energy in hydrogen fuel.

Recent research mainly focuses on proton exchange membrane (PEM) electrolysis technology, because it has advantages over alkaline electrolyzer cells, such as higher current density, higher hydrogen purity, non-hazardous liquid electrolyte, faster transient response, lower energy consumption, direct hydrogen storage and easy maintenance[1-6]. Despite the above-mentioned advantages, the efficiency of PEM electrolysis is still not satisfactory, due to high activation losses at the electrodes, especially at the oxygen electrode. An effective method to improve the performance of proton exchange membrane electrolyzer cell (PEMEC) is to operate PEMEC at higher temperatures [7-10]. The operating temperature of high temperature PEM electrolyzer cell is generally higher than 100℃ but below 180℃. As the ohmic losses of the electrolyte and the activation losses of the electrode both decrease with increasing temperature, the higher operating temperature can significantly reduce the overpotentials of the electrolyzer, improving the electrolyzer efficiency. Furthermore, the Gibbs free energy change decreases with increasing temperature, the electric energy demand for electrolysis is decreased.

Actually, more electric energy demand is replaced by thermal energy input at a higher temperature, making the high temperature electrolysis suitable to utilize waste heat from the industries. Another important feature of the modelling HT-PEMEC is that the water in the HT-PEMEC is in the gas phase, significantly simplifying water-gas management [11].

Considering the above advantages, it is very important to develop models to understand the physical-chemical processes in the electrolyzer cells and to optimize the structural and operational parameters of the electrolyzer cells. Despite much experimental research on HT-PEMECs, only a few modeling studies are available in the literature. Dale et al. [12] proposed a semi-empirical model, using regression analysis and curve fitting of polarization curve. Their results showed that the exchange current density of the electrodes and conductivity of the membrane increased with increasing temperature. S.Toghyani et al. [13] developed a 3D model to investigate the influences of temperature, pressure and structural parameters on the performance of an HT-PEMEC. Their results indicated that the temperature and pressure were the most significant parameters but the thickness and porosity of gas diffusion layer had no significant effect on the electrolyzer performance. S.Toghyani et al. [14] proposed a finite volume numerical method for exergoeconomic analysis and simulation of an HT-PEMEC. It was found that the performance of the high temperature PEM electrolyzer cell decreased with increasing pressure at voltage below 1.4V and electrolyzer cell operating at higher pressures could reduce the exergy cost of hydrogen. Onda et al. [15] established a 2D model for the PEM electrolyzer cell. They utilized an empirical formula based on temperature and current density to study the electrochemical reaction, but the thermal field was not analyzed. Han et al. [16]

proposed an ohmic loss model for PEM electrolytic cells. They studied the effects of different operating and structural parameters, including pressure, temperature, exchange current density, membrane thickness, electrode thickness, and inter-surface resistance on the performance of PEM electrolyzer cell. It was found that the electrolyzer performance could be improved by increasing temperature. However, the increase in pressure and membrane thickness had a negative effect on the performance of the electrolyzer cell. Tijani et al. [17] proposed a CFD model to study the flow field on the anode side of the PEM electrolyzer. The results show that the pressure gradient decreases along the bipolar plate, and the uniformity of the pressure gradient mainly depends on the design of the flow field of the bipolar plate.

These studies mainly study the operating parameters and structural parameters of high-temperature PEM electrolyzer cells, most of the models are steady-state. The dynamic response of the HT-PEMEC in the start-stop and adjustment phase is critical for practical application, but they are rarely studied at present. To fill in this research gap, this article proposed a safe and fast dynamic response scheme, and form a good basis for subsequent stack-level and system-level dynamic study and control.

2. Model description

The 2D multi-physics model is developed to investigate the dynamic response of HT-PEMEC, including electrochemical reaction, heat transport, mass and momentum transport. As shown in Fig.1, the four types of control volume are used in the dynamic model such as gas channel, gas diffusion layer (GDL), catalyst layer (CL) and membrane [18]. Within these control volumes, the transport processes of heat, mass and momentum are determined by the

conservation laws.

Following major assumptions is employed for the model:

1) All material parameters are homogeneous and isotropic.

2) The gas species is considered as an ideal gas, and the gas flow is laminar in gas channels.

3) The distribution of the reaction site is uniform in the catalyst layer, while the electrolysis reactions are not uniform in the catalyst layer. The highest reaction rate at the electrode-electrolyte interface, but that decreases significantly with increasing distance away from this interface.

2.1 Electrochemical model

The applied voltage (V_{cell}) corresponds to the sum of the Nernst voltage (V_{Nernst}) and the overpotential losses in an HT-PEMEC as shown in Eq.(1). The overpotential losses include activation overpotentials (η_{act}) and Ohmic overpotentials (η_{ohm}), which generally generate heats.

$$V_{cell} = V_{Nernst} + \eta_{act} + \eta_{ohm} \tag{1}$$

The Nernst voltage of the electrolysis reaction includes concentration polarization because the gas partial pressures at the triple phase boundary (TPB) are used instead of the gas partial pressure at the electrode surface [19].

$$V_{Nernst} = E^0_{H_2} + \frac{RT}{2F} ln \left[\frac{P^L_{H_2} \left(P^L_{O_2}\right)^{1/2}}{P^L_{H_2O}} \right] \tag{2}$$

Where R is the universal gas constant and T operating temperature. $E^0_{H_2}$ represents the equilibrium potential under standard conditions. F is the Faraday constant. $P^L_{H_2}$, $P^L_{H_2O}$, and$P^L_{O_2}$

represent the local partial pressures of H_2, H_2O, and O_2 at TPB, respectively.

The activation polarization of the electrolysis reaction involves energy barriers that needs to be overcome by the reacting species. The relationship between the current density and activation polarization is commonly expressed by the Butler-Volmer equation:

$$\mathrm{i} = i_0 \left\{ exp\left(\frac{\alpha n F \eta_{act}}{RT}\right) - exp\left(\frac{(1-\alpha) n F \eta_{act}}{RT}\right) \right\} \quad (3)$$

where α is the transfer coefficient and i_0 the exchange current density. i represent the operating current density. n denotes the number of transferred electrons of electrolysis reaction.

Ohmic polarization occurs according to the flow of proton and electronic in HT-PEMEC, which can be calculated by Ohm's law. The detailed information for the calculation process can be found in Ref. [20-21].

2.2 mass and momentum transport model

Transport of gaseous species is considered for free molecular diffusion and Knudsen diffusion in the porous electrode, while only free molecular diffusion is considered in gas channels. The mass transport process can be described by the general Fick's model [22].

$$N_i = -\frac{1}{RT}\left(\frac{B_0 y_i P}{\mu}\nabla P - D_i^{eff}\nabla(y_i P)\right) \text{ (i=1,2,…..n)} \quad (4)$$

Where N_i is defined as the flux of mass transport, y_i is the mole fraction of component i and B_0 the permeability coefficient. μ and D_i^{eff} represent gas viscosity and the effective diffusivity of species i, respectively. Further, the D_i^{eff} can be expressed as [23]:

$$D_i^{eff} = \frac{\varepsilon}{\tau}\left(\frac{1}{D_{im}^{eff}} + \frac{1}{D_{ik}^{eff}}\right) \quad (5)$$

Where ε is the porosity of porous material and τ tortuosity. D_{im}^{eff} and D_{ik}^{eff} depend on the structure of porous material, and more detailed can be found in Ref. [24].

The momentum transport process is described by the Navier-Stokes (N-S) equation, and can be shown as Eq. (6) in the gas channels:

$$\rho\frac{\partial \mathrm{u}}{\partial \mathrm{t}} + \rho \mathrm{u}\nabla \mathrm{u} = -\nabla \mathrm{p} + \nabla\left[\mu(\nabla \mathrm{u} + (\nabla \mathrm{u})^T) - \frac{2}{3}\mu\nabla \mathrm{u}\right] \quad (6)$$

For porous electrodes, the N-S equation with Darcy's term is used to describe the momentum transport [25]:

$$\rho\frac{\partial \mathrm{u}}{\partial \mathrm{t}} + \rho \mathrm{u}\nabla \mathrm{u} = -\nabla \mathrm{p} + \nabla\left[\mu(\nabla \mathrm{u} + (\nabla \mathrm{u})^T) - \frac{2}{3}\mu\nabla \mathrm{u}\right] - \frac{\varepsilon\mu \mathrm{u}}{B_0} \quad (7)$$

where u is gas flow rate and ρ gas density. p represents operating pressure.

2.3 heat transfer model

The electrolysis reaction is endothermic while the irreversible losses are exothermic [26]. The heat transfer process can be described by the general heat balance equation.

$$\rho C_p u \bullet \nabla T + \nabla\left(-\lambda_{eff}\nabla T\right) = Q \quad (8)$$

where C_p represents fluid heat capacity and u is fluid velocity. λ_{eff} is the effective thermal conductivity. Q is the heat source, which generates or consumes heats due to irreversible losses or the electrochemical reaction. Further, λ_{eff} can be calculated by Eq.(9) at the porous material [27].

$$\lambda_{eff} = (1-\varepsilon)\lambda_s + \varepsilon\lambda_g \quad (9)$$

Where λ_s is the solid thermal conductivity and λ_g is gaseous thermal conductivity. Table 1 shows the value of the operating parameters and structural parameters used in the simulation.

Table 1. Parameters used in the model validation.

Parameter	value	unit
Channel length	20	mm

Channel height	1	mm
Gas diffusion layer thickness	0.38	mm
Gas diffusion layer length	20	mm
Catalyst layer thickness	0.05	mm
Catalyst layer length	20	mm
Membrane thickness	0.1	mm
Membrane length	20	mm
Operating temperature	403.15	K
Operating pressure	1	bar
Porosity of catalyst layer	0.3	
GDL porosity	0.4	
Electrode permeability	2.36×10^{-12}	m^2
GDL permeability	1.18×10^{-11}	m^2
Anode transfer coefficient	10^{-4}	A/cm^{-2}
Cathode transfer coefficient	0.1	A/cm^{-2}
Anode exchange current	0.2	
Cathode exchange current	0.5	
Proton conductivity of electrolyte	20	S/m

2.4 Boundary conditions and model solution

The electric potential is specified on the outer surfaces of the cathode and anode. However, both ends of the cathode and anode are insulated. The gas flow rate, gas mass fraction and gas temperature are given at the inlet, and the pressure is given at the outlet.

The dynamic model is solved at given operating parameters and structural parameters such as temperature, operating voltage, gas mole fraction and gas flow rate. The transient solver with newton nonlinear method is used, and the time step is set to 0.01s. The commercial software COMSOL MULTIPHYSICS® is used for dynamic simulation.

3. Results and discussion

3.1 Model validation

In this section, the model is verified by comparing experimental results [28] and simulation datum. Fig.2 shows the current-voltage curves of experimental results and

simulation datum. It is found that the small error between the modelling results and experimental datum are observed, which validates the developed model.

3.1 initial steady state and thermal safety

The cathode gas flow rate, anode gas flow rate and anode gas mass fraction are discretized to determine the maximum efficiency points at different voltages. The dynamic adjustment of the system is usually the adjustment process from one maximum efficiency point to another maximum efficiency point. The efficiency of HT-PEMEC is defined as the ratio of the total energy output to the total energy input. The total energy inputs include two parts. One part of the energy input is the electrical energy, and the other part of energy input is used to heat input gas. The total energy output is the heat of the hydrogen produced.

$$\eta = \frac{(\dot{m}_{o,H_2} - \dot{m}_{i,H_2}) LHV_{H_2}}{V \int_0^{L_{RU}} i dz + \dot{m}_{i,ca} \int_{T_0}^{T_{i,ca}} C_{p,g,ca} dT + \dot{m}_{i,an} \int_{T_0}^{T_{i,an}} C_{p,g,an} dT} \tag{10}$$

Here $\dot{m}_{o,H_2}$ and $\dot{m}_{i,H_2}$ are defined as the hydrogen mass flow rate per unit area of inlet and outlet. $\dot{m}_{i,ca}$ and $\dot{m}_{i,an}$ represent the inlet gas mass flow rate per unit area of anode and cathode. $C_{p,g,ca}$ and $C_{p,g,an}$ are the heat capacity of the anode and cathode. L_{RU} denotes the channel width. The ambient temperature T_0 is specified at 303.15 K and the lower heating value (LHV) of hydrogen is employed for the metrics [29].

Table 2 shows the maximum efficiency points and these points can be used as an initial steady state to study dynamic processes. The model initial steady state is set as the maximum efficiency point at 1.5V.

Table 2. Maximum efficiency points at different voltages.

Applied voltage	Cathode gas flow rate	Anode gas flow rate	Anode water mass fraction	efficiency
1.5 V	0.03 m s^{-1}	0.03 m s^{-1}	0.30	32.9%
1.6 V	0.05 m s^{-1}	0.03 m s^{-1}	0.30	47.1%
1.7 V	0.08 m s^{-1}	0.03 m s^{-1}	0.41	53.7%
1.8 V	0.13 m s^{-1}	0.03 m s^{-1}	0.42	54.2%

In order to reduce damage probability and increase the lifetime of HT-PEMEC, the temperature gradient is considered for thermal safety. The excessive temperature gradient along the gas channel will lead to cell degradation and thermal cracking [30]. Zhang et al. limited the temperature gradient along the flow direction to be less than 800 K m^{-1} [31]. Here, temperature gradient of the model is limited to less than 500 K m^{-1}.

3.2 Dynamic response constraints

The dynamic response of HT-PEMEC is usually slow and can be divided into two main processes. Electrochemical response dominates in the first process, which is faster than the subsequent temperature response process. The dynamic response is an open loop based on the model, and some significant constraints will limit the process of dynamic switching as summarized below:

1) The overall response process is mainly limited by the slow temperature response.

2) An excessive temperature gradient can cause irreversible damage.

3) Fuel starvation problem during dynamic response process.

Based on these three constraints, the goal of dynamic switching is as fast as possible.

3.3 Dynamic response process

To investigate the dynamic process, three different dynamic switching methods are first compared, including step scheme, multistep scheme, and diagonal scheme. Fig.3 shows detailed information about the three different switching scheme.

1) Step scheme: The step function is used for voltage regulation, resulting in fast switching from low to high voltages.

2) Multistep scheme: The voltage regulation uses a step function multiple times.

3) Diagonal scheme: Slower voltage regulation with a constant rate.

The assumptions for these three different dynamic switching schemes are as follows. The step scheme has a step signal with an amplitude of 0.2 V at the 2^{nd} second. In the multi-step scheme, from the 2^{nd} second to the 6^{th} second, a step signal with a value of 0.04 V is given every second. In the diagonal scheme, the voltage signal is set to a slope of 0.05 V/s, and the multistep scheme has the same adjustment time with the diagonal scheme. Except for the voltage switching mode, switching schemes of the cathode flow rate, anode flow rate and anode steam mass fraction are same.

The dynamic responses of three different switching schemes are compared. Fig.4a presents the current density response of three different switching schemes. Here, the dynamic response of current density is mainly affected by the electrolyte potential and temperature. The difference in response time between the cell potential and the operation temperature results in a positive overshoot, which was also observed in ref. [32] on high temperature solid oxide electrolyzer cell (SOEC). The dynamic response of the electrolyte potential is very fast while

the dynamic response of temperature is very slow. Fig.4b and Fig.4c show the dynamic responses of average electrolyte potential and average temperature, respectively. Therefore, the current density response is mainly affected by the electrolyte potential in the initial stage, which is also the main reason for the overshoot, and then the current density is mainly affected by the operating temperature. The step scheme has a fast current density dynamic response, but excessive overshoot is a problem that should be avoided in the control process. For comparison, the overshoot of the diagonal scheme is the smallest, and the dynamic response of the multistep scheme is the slowest. Fig.4d and Fig.4e show heat generation and consumption due to overpotential loss and electrochemical reactions. Activated overpotential accounts for the main part of overpotential loss, so overpotential loss is almost proportional to current density. Besides, the heat generation due to overpotential loss is greater than the heat consumption due to the electrochemical reaction, which is the main reason for the increase in operating temperature. Fig.4f shows the different temperature gradient dynamic processes in three different schemes. The temperature gradient dynamic process of the step scheme is faster, and the temperature gradient dynamic process of the multi-step scheme and the diagonal scheme is not much different. From the perspective of thermal safety, the temperature gradient of the three schemes is within 500 K m^{-1}, which belongs to the thermal safety range. Hydrogen flux at the outlet of the gas flow channel is shown in Fig.4g. The hydrogen flux at the outlet is almost linearly related to the current density, because the amount of hydrogen produced is linearly related to the current density.

3.4 Reactants starvation

Another major limitation on dynamic response is reactants starvation. When the problem of reactants starvation occurs on the anode side, the anode catalyst is oxidized, causing irreversible damage to the electrolyzer. Fig.5a shows the transient response of the minimum anode steam mole fraction at the electrode-electrolyte interface. Because mass transfer is slower than charge transfer, rapid and large change of current density cause a significant downward trend of the minimum steam mole fraction in the initial stage. In contrast, due to the slower current density response of the multi-step scheme and the diagonal scheme, there is no similar trend. Fig.5b represents the dynamic response of minimum anode steam mole fraction on different step responses. The greater the magnitude of the voltage step response, the more obvious the downward trend of the minimum mole fraction of anode steam, which is more likely to cause the problem of reactant starvation. In terms of preventing reactant starvation, the diagonal scheme is more advantageous.

3.5 Dynamic process optimization

The diagonal scheme has the obvious advantage of fast dynamic and prevents reactant exhaustion. However, as the slope increases, the minimum reactant concentration shows a sudden downward trend at the electrode-electrolyte interface. Fig.6a shows the transient response of minimum anode steam mole fraction on different slope. In order to prevent the obvious downward trend of the minimum steam mole fraction during the dynamic response, the constraint condition is specified, which the minimum anode steam mole fraction cannot be less than 5% of that in the final steady state. When the voltage growth rate of the diagonal

scheme reaches 0.4, it not only satisfies the constraint condition but also has a faster dynamic response. However, by optimizing the dynamic process, not only can the problem of reactant exhaustion be prevented, but the response speed is faster than the diagonal scheme.

The dynamic optimization scheme is shown in Fig.6b. The optimization dynamic process is divided into t_1 stage and t_2 stage. The t_1 stage is the main phase of the dynamic process, which voltage change rate is fast and the dynamic process changes drastically. In the t_2 stage, the system finally reaches the desired steady state. The voltage change rate is relatively slow in this stage, which can effectively suppress the overshoot of the dynamic process.

Fig.7 shows the effect of different voltage change rates K_1 and K_2 on the dynamic process. In this process, the t_1 phase and the t_2 phase remain equal and unchanged. The influence of the voltage change rate on the dynamic process is explored by changing K_1 and K_2. The minimum mole fraction of anode steam decreases with increasing K_1, as more steam is consumed in the initial stage with a larger K1. Furthermore, the increase in voltage change rate K_1 leads to a decrease in K_2, which reduces the overshoot of the dynamic process and reaches a steady state faster.

Fig.8 shows the effect of different t_1 and t_2 on the dynamic process. In this process, the final steady state and the voltage change rate K_1 remain unchanged, and the effect of the difference in the time periods t_1 and t_2 on the dynamic process is studied. Since the voltage change rate is more drastic in the time period t_1, the increase in the time period t_1 leads to a decrease in the minimum mole fraction of anode steam, which is more likely to cause the problem of reactant starvation. On the other hand, an increase in the period t_1 reduces the

voltage change rate K_2, which reduces the response time and overshoot during dynamics process.

The dynamic optimization of this model is determined by the parameters K_1 and t_1. Both an excessive voltage change rate K_1 and an excessively long time period t_1 can cause the problem of reactant starvation. The feasible region for dynamic process optimization is found by limiting the minimum steam mole fraction. Fig.9a shows the area enclosed by the solid line and the dotted line is the feasible region. When the slope is 0.4, it is the slope scheme, so the solution on the dotted line is not included.

The solution in the feasible domain has a faster dynamic process than the diagonal scheme and can prevent the problem of reactant starvation. Fig.9b shows the dynamic response of efficiency. In the dynamic process, the efficiency of the dynamic process optimization is slightly greater than the diagonal scheme. Because the input energy is almost the same, but the current density response of the optimization process is faster, so the optimization process produces more hydrogen and makes higher efficiency. The greater K_1 or t_1, the better the dynamic performance, but too large K_1 and t_1 may exceed the constraint of the minimum steam mole fraction.

4. Conclusions

In this paper, a 2D multi-physics model is developed to study the dynamic process of different schemes. The dynamic response process of step scheme is fastest, but it is easy to cause the problem of reactant starvation. The dynamic response of the diagonal scheme is faster and can prevent the problem of reactant starvation. Subsequently, the dynamic process is optimized. The voltage signal is divided into a t_1 stage with a larger voltage growth rate K_1 and

a t_2 stage with a slower voltage growth rate K_2. It is found that when t_1 and t_2 remain unchanged, the larger K_1 is, the smaller the minimum mole fraction of water steam in the dynamic process. The smaller K_2, the faster the dynamic response speed and the smaller the overshoot. It is found that when K_1 is unchanged, the longer the t_1 time period, the smaller the minimum steam mole fraction in the dynamic process, the smaller the overshoot, the faster the dynamic response speed. The values of t_2 and K_2 can be determined according to the values of t_1 and K_1. t_1 and K_1 are used as the vector space, and the minimum water steam mole fraction is used as the constraint condition in the dynamic process to find the feasible region. Solutions in the feasible domain have better dynamic performance than diagonal schemes.

Acknowledgement

M. Ni thanks the funding support from The Hong Kong Polytechnic University (G-YW2D) and grants (Project Number: PolyU 152214/17E and PolyU 152064/18E) from Research Grant Council, University Grants Committee, Hong Kong SAR.

References

[1] Tijani AS, Rahim AHA. Numerical modeling the effect of operating variables on Faraday efficiency in PEM electrolyzer. Procedia Technol 2016;26:419-27.

[2] dos Santos KG, Eckert CT, De Rossi E, Bariccatti RA, Frigo EP, Lindino CA, et al. Hydrogen production in the electrolysis of water in Brazil, a review. Renew Sustain Energy Rev 2017;68:563-71.

[3] Wang M, Wang Z, Gong X, Guo Z. The intensification technologies to water electrolysis for hydrogen production-A review. Renew Sustain Energy Rev 2014;29:573e88.

[4] Buttler A, Spliethoff H. Current status of water electrolysis for energy storage, grid balancing and sector coupling via power-to-gas and power-to-liquids: a review. Renew Sustain Energy Rev 2017;82:2440e54.

[5] Carmo M, Fritz D L, Mergel J, et al. A comprehensive review on PEM water electrolysis[J]. International journal of hydrogen energy, 2013, 38(12): 4901-4934.

[6] Grigoriev S A, Porembsky V I, Fateev V N. Pure hydrogen production by PEM electrolysis for hydrogen energy[J]. International Journal of Hydrogen Energy, 2006, 31(2): 171-175.

[7] Nikiforov A V, García A L T, Petrushina I M, et al. Preparation and study of IrO2/SiC–Si supported anode catalyst for high temperature PEM steam electrolysers[J]. International Journal of Hydrogen Energy, 2011, 36(10): 5797-5805.

[8] Nikiforov A V, Petrushina I M, Christensen E, et al. WC as a non-platinum hydrogen evolution electrocatalyst for high temperature PEM water electrolysers[J]. International journal of hydrogen energy, 2012, 37(24): 18591-18597.
[9] Nikiforov A, Christensen E, Petrushina I, Jensen JO, Bjerrum NJ. Advanced construction materials for high temperature steam PEM electrolysers. INTECH Open Access Publisher; 2012.
[10] Hansen MK, Bjerrum N, Christensen E, Jensen JO. PEM water electrolysis at elevated temperatures. Ph.D. thesis. Technical University of Denmark, Department of Chemistry Institut; 2012.
[11] Aili D, Hansen MK, Pan C, Li Q, Christensen E, Jensen JO, et al. Phosphoric acid doped membranes based on Nafion®, PBI and their blends-Membrane preparation, characterization and steam electrolysis testing. Int J Hydrogen Energy 2011;36:6985-93.
[12] Dale NV, Mann MD, Salehfar H. Semiempirical model based on thermodynamic principles for determining 6kW proton exchange membrane electrolyzer stack characteristics. J Power Sources 2008;185:1348-53.
[13] Toghyani S, Afshari E, Baniasadi E, et al. Thermal and electrochemical performance assessment of a high temperature PEM electrolyzer. Energy, 2018, 152: 237-246.
[14] Toghyani S, Baniasadi E, Afshari E. Numerical simulation and exergoeconomic analysis of a high temperature polymer exchange membrane electrolyzer[J]. International Journal of Hydrogen Energy, 2019, 44(60): 31731-31744.
[15] Onda K, Murakami T, Hikosaka T, Kobayashi M, Ito K. Performance analysis of polymer-electrolyte water electrolysis cell at a small-unit test cell and performance prediction of large stacked cell. J Electrochem Soc 2002;149:A1069-78.
[16] Han B, Steen SM, Mo J, Zhang F-Y. Electrochemical performance modeling of a proton exchange membrane electrolyzer cell for hydrogen energy. Int J Hydrogen Energy 2015;40:7006-16.
[17] Tijani AS, Barr D, Rahim AHA. Computational modelling of the flow field of an electrolyzer system using CFD. Energy Procedia 2015;79:195-203.
[18] Ruiz D D H, Sasmito A P, Shamim T. Numerical investigation of the high temperature PEM electrolyzer: effect of flow channel configurations. ECS Transactions, 2013, 58(2): 99-112.
[19] Nafchi F M, Baniasadi E, Afshari E, et al. Performance assessment of a solar hydrogen and electricity production plant using high temperature PEM electrolyzer and energy storage[J]. International Journal of Hydrogen Energy, 2018, 43(11): 5820-5831.
[20] Xu H, Chen B, Irvine J, et al. Modeling of CH4-assisted SOEC for H2O/CO2 co-electrolysis. International Journal of Hydrogen Energy, 2016, 41(47): 21839-21849.
[21] Ni M. 2D thermal modeling of a solid oxide electrolyzer cell (SOEC) for syngas production by H2O/CO2 co-electrolysis. International Journal of Hydrogen Energy, 2012; 37(8): 6389-6399.
[22] Suwanwarangkul R, Croiset E, Fowler MW, Douglas PL, Entchev E, Douglas MA. Performance comparison of Fick's, dusty-gas and StefaneMaxwell models to predict the concentration overpotential of a SOFC anode. J Power Sources 2003;122:9-18.
[23] Chan SH, Khor KA, Xia ZT. A complete polarization model of a solid oxide fuel cell and its sensitivity

to the change of cell component thickness. J Power Sources 2001;93:130-40.
[24] Todd B, Young JB. Thermodynamic and transport properties of gases for use in solid oxide fuel cell modelling. J Power Sources 2002;110:186-200.
[25] Kakaç S, Pramuanjaroenkij A, Zhou XY. A review of numerical modeling of solid oxide fuel cells. Int J Hydrogen Energy 2007;32:761-86.
[26] Xu H, Chen B, Zhang H, et al. The thermal effect in direct carbon solid oxide fuel cells. Applied Thermal Engineering, 2017, 118: 652-662.
[27] He Q, Yu J, Xu H, et al. Thermal effects in H2O and CO2 assisted direct carbon solid oxide fuel cells[J]. International Journal of Hydrogen Energy, 2020.
[28] Hansen M K, Aili D, Christensen E, et al. PEM steam electrolysis at 130° C using a phosphoric acid doped short side chain PFSA membrane. International Journal of Hydrogen Energy, 2012, 37(15): 10992-11000.
[29] Luo Y, Shi Y, Li W, et al. Comprehensive modeling of tubular solid oxide electrolysis cell for co-electrolysis of steam and carbon dioxide. Energy, 2014, 70: 420-434.
[30] A. Amiri, S. Tang, P. Vijay, M.O. Tadé, Planar solid oxide fuel cell modeling and optimization targeting the stack's temperature gradient minimization, Ind. Eng. Chem. Res. 55 (27) (2016) 7446-7455.
[31] L. Zhang, X. Li, J. Jiang, S. Li, J. Yang, J. Li, Dynamic modeling and analysis of a 5- kW solid oxide fuel cell system from the perspectives of cooperative control of thermal safety and high efficiency, Int. J. Hydrogen Energy 40 (1) (2015) 456–476.
[32] Udagawa J, Aguiar P, Brandon N P. Hydrogen production through steam electrolysis: Model-based dynamic behaviour of a cathode-supported intermediate temperature solid oxide electrolysis cell[J]. Journal of Power Sources, 2008, 180(1): 46-55.

Figure captions

Fig.1 Schematic view of the high temperature PEM electrolyzer.

Fig.2 HT-PEMECs model validated with experimental results.

Fig.3 Operating parameters under different dynamic scheme.

Fig.4 Dynamic response of current density (a), average electrolyte potential (b), average temperature (c), temperature gradient (d) and hydrogen flux at the outlet (e).

Fig.5 (a) Dynamic response of minimum anode steam mole fraction; (b) The minimum anode steam mole fraction under different step responses.

Fig.6 (a) Dynamic response with different slopes; (b) Dynamic optimization scheme.

Fig.7 Effect of K_1 and K_2 on dynamic process.

Fig.8 Effect of t_1 and t_2 on dynamic process.

Fig.9 (a) The feasible region of optimization problem; (b) Dynamic response of efficiency.

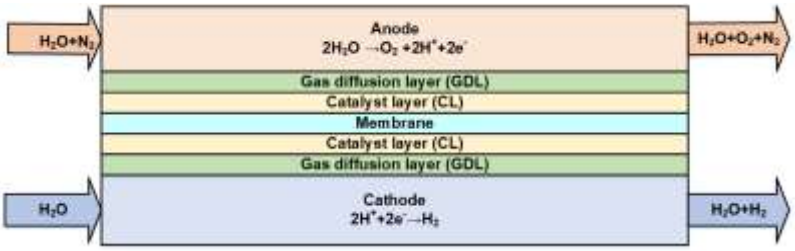

Fig.1 Schematic view of the high temperature PEM electrolyzer.

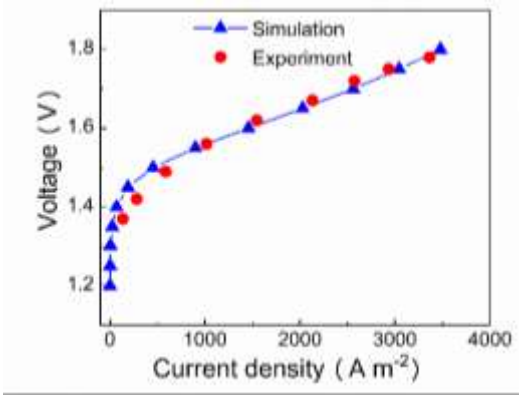

Fig.2 HT-PEMECs model validated with experimental results.

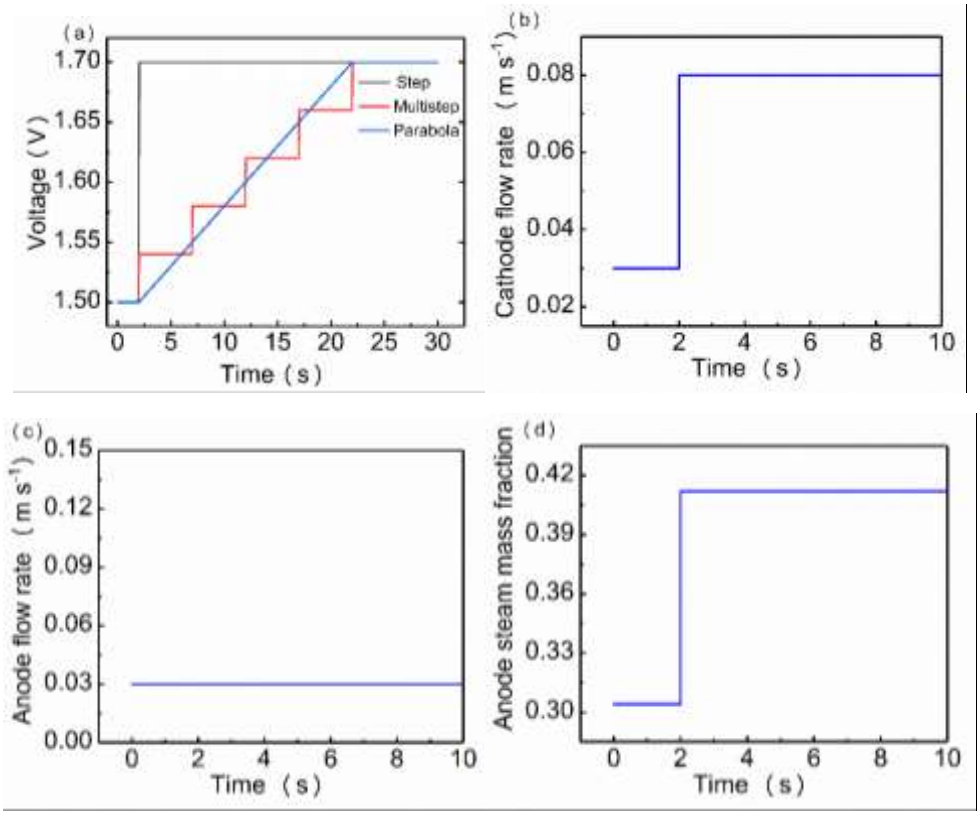

Fig.3 Operating voltage (a), cathode flow rate (b), anode flow rate (c) and anode steam mass (d) under different dynamic schemes.

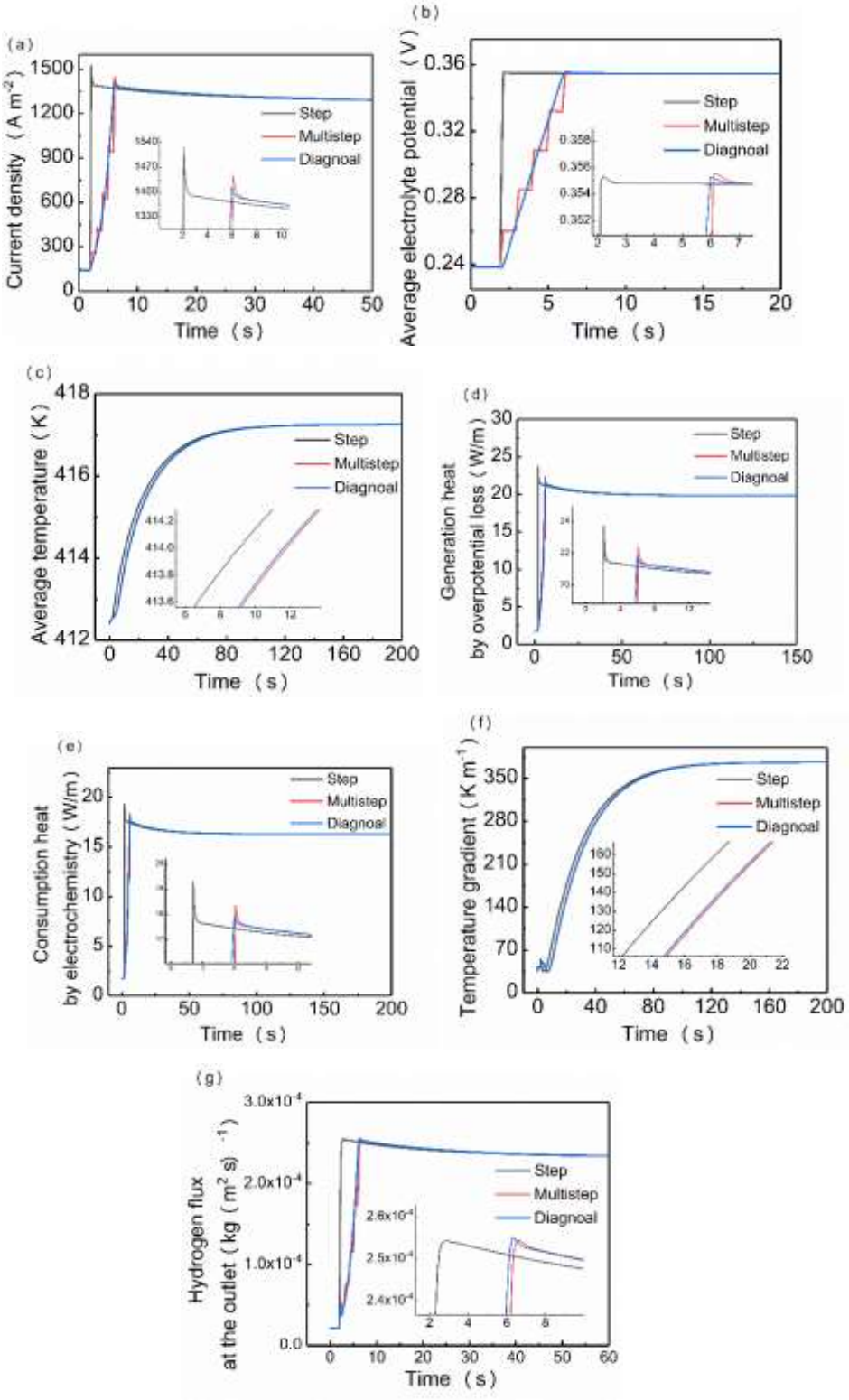

Fig.4 Dynamic response of current density (a), average electrolyte potential (b), average temperature (c), generation heat by overpotential loss (d), consumption heat by electrochemistry (e), temperature gradient (f) and hydrogen flux at the outlet (g).

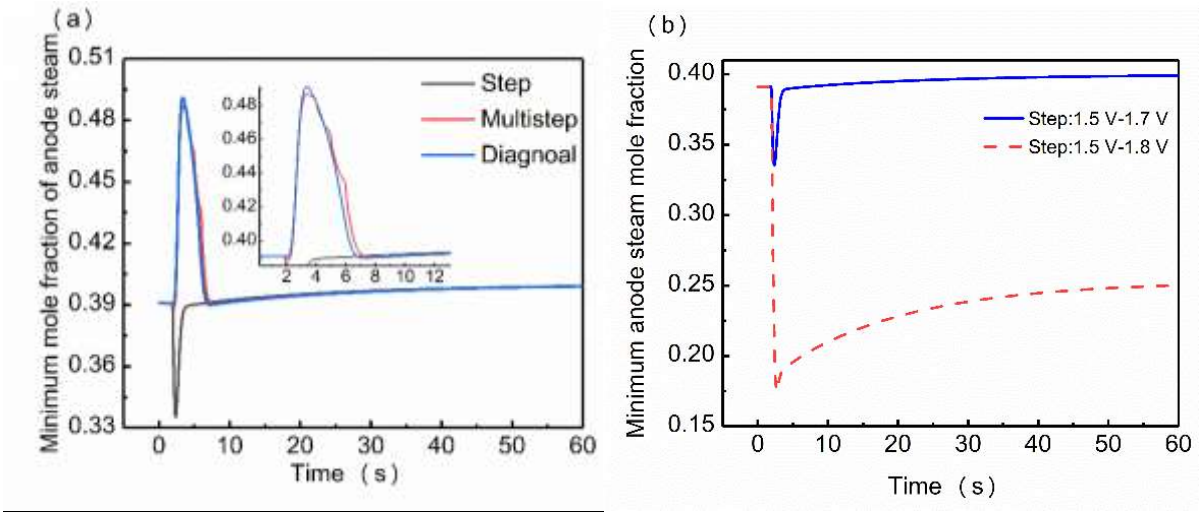

Fig.5 (a) Dynamic response of minimum anode steam mole fraction; (b) The minimum anode steam mole fraction under different step responses.

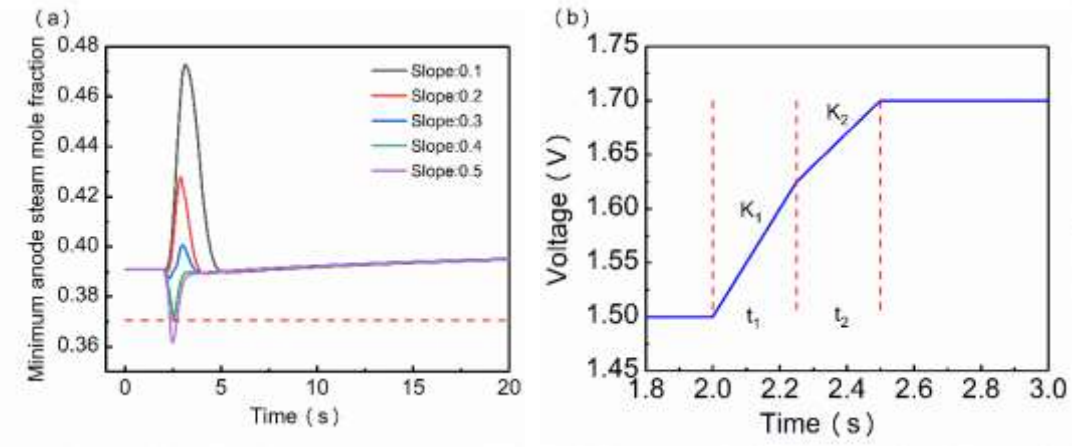

Fig.6 (a) Dynamic response with different slopes; (b) Dynamic optimization scheme.

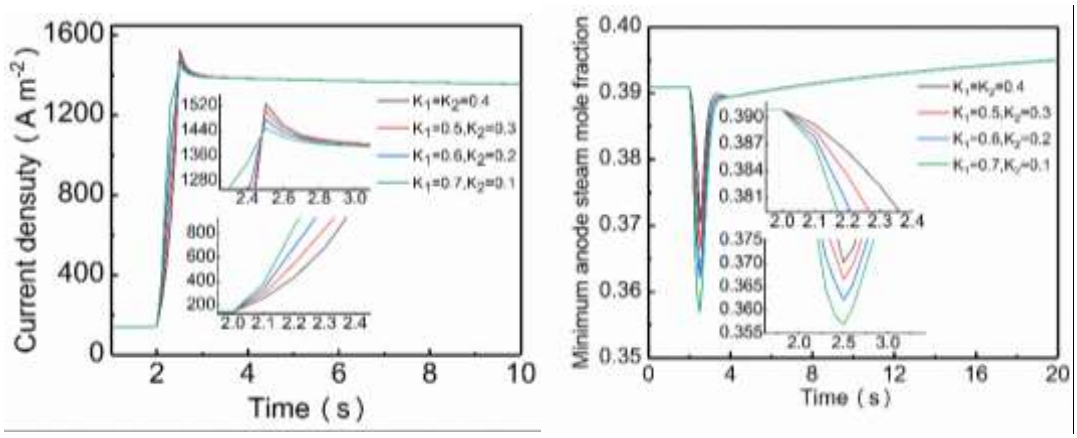

Fig.7 Effect of K_1 and K_2 on dynamic process.

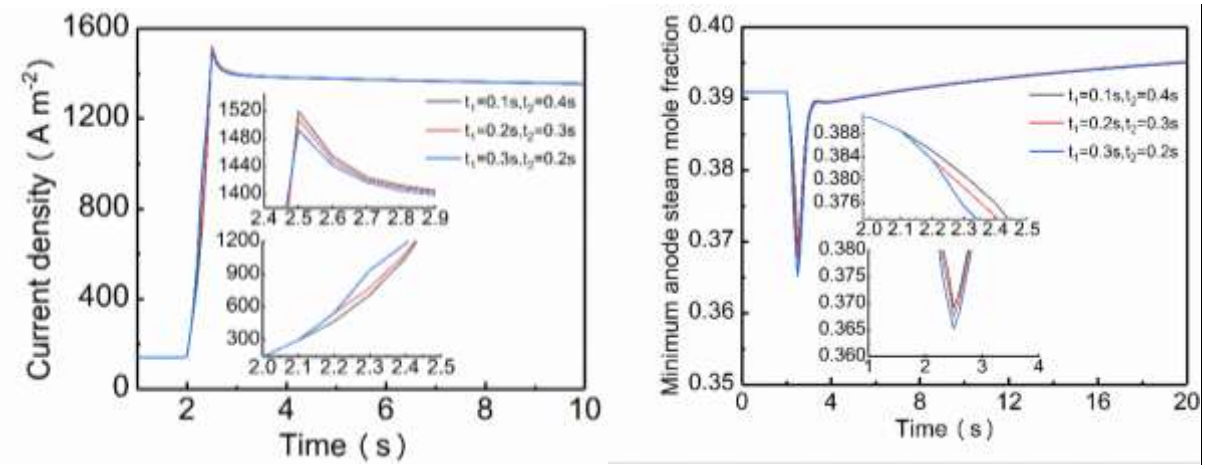

Fig.8 Effect of t_1 and t_2 on dynamic process.

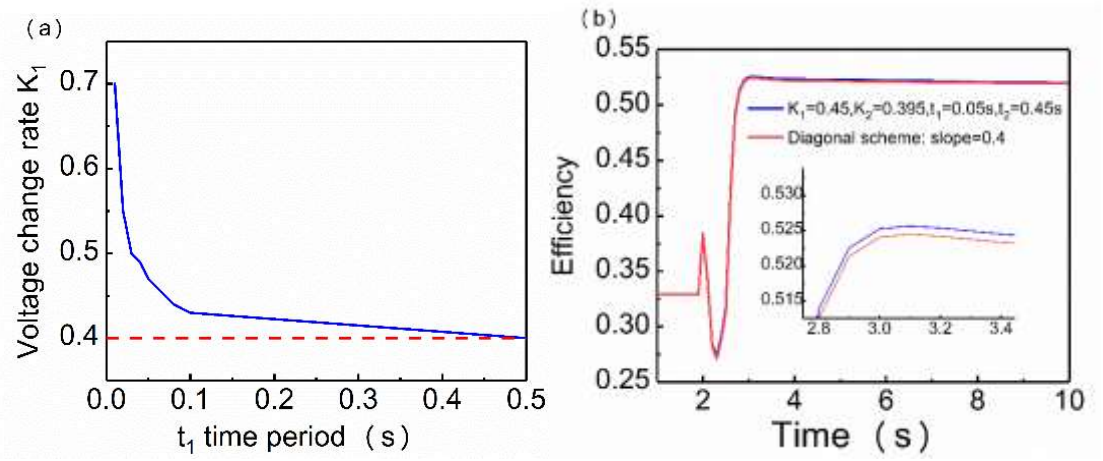

Fig.9 (a) The feasible region of optimization problem; (b) Dynamic response of efficiency.